

## RESEARCH ARTICLE

## Luminescence feature of new 3,6-di(thiazolidin-5-one-2-yl)-carbazole derivative: synthesis, photophysical properties, density functional theory studies, and crystal shape effect

Tahani M. Bawazeer<sup>1</sup> | Ismail Althagafi<sup>1</sup>  | Moataz Morad<sup>1</sup> | Alaa M. Munshi<sup>1</sup> | Abrar A. Bayazeed<sup>1</sup> | Arwa Alharbi<sup>1</sup> | Nashwa El-Metwaly<sup>1,2</sup> <sup>1</sup>Department of Chemistry, College of Applied Sciences, Umm Al-Qura University, Makkah, Saudi Arabia<sup>2</sup>Chemistry Department, Faculty of Science, Mansoura University, Mansoura, Egypt

## Correspondence

Nashwa El-Metwaly, Chemistry Department, College of Applied Sciences, Umm Al-Qura University, 21955, Makkah, Saudi Arabia.  
Email: n\_elmetwaly00@yahoo.com; nmmohamed@uqu.edu.sa

## Abstract

A new carbazole chromophore conjugated with substituted thiazolidine-4-one (CzPT) was synthesized by applying the Knoevenagel reaction between 3,6-diformyl-*N*-hexylcarbazole and ethyl 2-aceto-2-(5-oxo-3-phenylthiazolidin-2-ylidene)acetate. The chemical structure of the new derivative (CzPT) was elucidated by spectral studies. The CzPT absorption spectra in different solvents exhibited a red shift for  $\lambda_{\max}$  by increasing solvent polarity. Bands at 430–474 nm appeared and were attributed to intramolecular charge transfer with high  $\pi$ - $\pi^*$  characteristics. CzPT fluorescence spectra exhibited a red shift after increasing the solvent polarity. To understand the Stokes' shift ( $\Delta\bar{\nu}$ ) behaviour of the CzPT derivative referring to the polarity of solvents, Lippert–Mataga and linear solvation-energy relationship (LSER) models were employed in which the LSER exhibited respectable results compared with Lippert–Mataga ( $r^2 = 0.9707$ ). Moreover, time-dependent density functional theory absorption spectra in hexane and dimethylformamide showed that  $\lambda_{\max}$  had a major contribution in the highest occupied molecular orbital to lowest unoccupied molecular orbital transition in both solvents. In addition, the reduced uniformity of crystal features may lead to dislocation or anomalous arrangement of crystals with irregular spacing, which automatically enhances the optical properties of such crystals.

## KEYWORDS

carbazole, DFT studies, energy gap, fluorescence, thiazolidine-5-one

## 1 | INTRODUCTION

Fluorescence systems have been used to investigate small molecules such as metal cations and other inorganic compounds.<sup>[1]</sup> Organic light-emitting diodes (OLEDs) have wide scope for improvement as highly efficient emitters.<sup>[2–4]</sup> The stability and emission of solid states remain a significant advantage for organic compounds used as OLEDs.<sup>[5,6]</sup> The sizable emission of combinations in solution usually develops low value in solid-state reactions due to electron transition and intermolecular energy,<sup>[7]</sup> therefore, the synthesis of compounds with high emission efficiency in the solid state, is important.<sup>[8]</sup> Donor-

acceptor compounds with a polyaromatic core have had much interest for use in electroluminescence (EL) devices due to their robust emissions in the solid state.<sup>[9]</sup> Understanding the structure of fluorescent compounds is important due to their wide application in the environment, biochemistry, and medical tenders, etc.<sup>[10–14]</sup> Many chemical and biochemical molecules such as gases, neutral molecules, anions and cations can be investigated using fluorescence techniques.<sup>[15,16]</sup> Poly(1-amino naphthalene) has been synthesized and used as a chemosensor to identify Fe<sup>3+</sup> via a fluorometric method.<sup>[17]</sup> Four fluorophores with a donor-acceptor structure with variable substitutions at the imidazole moiety have been synthesized.<sup>[18]</sup> Using waste

foam, S/N-carbon quantum dots have been synthesized and presented different colours such as blue, blue–green, green, green–yellow and yellow.<sup>[19]</sup> To date, despite the presence of a large number of fluorescent molecular sensors for specific applications, there is still an urgent need to prepare sensors with improved selectivity and small effects on the environment.<sup>[20,21]</sup>

In the absence of cations that may bind to the carbazole molecule, the electron–donor–acceptor (EDA) moiety displays charge transfer. Without complex formation via inorganic cations, the electron-donating capacity of electron donors decreases and the moiety does not reveal its charge transfer properties,<sup>[22–24]</sup> therefore absorption of the noncomplexed moiety is hypsochromically shifted compared with the complexed system.<sup>[25]</sup> Absorption of non-complexed systems produced a very weak hypsochromic shift in the fluorescence spectrum of the complexed moieties.<sup>[26]</sup> This can be explained as follows: after excitation the electron-donating moiety in the molecule is able to carry a positive charge, which results in fluorescence close to that of the noncomplexed system.<sup>[27]</sup> Charge transfer molecules with donor–acceptor moieties that bind by double bonds also often act as cation indicators.<sup>[28]</sup> Carbazole derivatives are good molecules for use in colour flat-panel displays.<sup>[29]</sup> Fluorescence compounds have diverse and specific applications such as in chemical sensors, biological detectors, and cosmic-ray detectors. Therefore, based on studies mentioned above, the goal of this research was to design and synthesize a new 3,6-di(thiazolidin-5-one-2-yl)-carbazole derivative that had fluorescence or optical properties. Such properties would allow it to have new applications, such as in special spectral and computer studies. The effects of crystal shape and shell thickness on the optical properties were also examined.

## 2 | EXPERIMENTAL

### 2.1 | General

Infrared spectra (KBr discs) were generated on a Thermo Scientific Nicolet iS10 FTIR spectrometer. <sup>1</sup>H nuclear magnetic resonance (NMR) (500 MHz) spectra were obtained using a JEOL's NMR spectrometer in deuterated chloroform (CDCl<sub>3</sub>). Mass spectroscopy was performed using a Shimadzu Qp-2010 Plus (GC–MS) spectrometer. The Unicam UV/Vis UV2 spectrometer was used to measure the electronic spectra in different solvents in 1 cm silica cells. The emission spectra were recorded on a PerkinElmer LS 55 fluorescence spectrometer.

### 2.2 | Synthesis of 9-hexyl-9H-carbazole-3,6-dicarbaldehyde (1)

To a two-necked round-bottomed (RB) flask, 100 ml, 15 ml of stirred solution of dry dimethyl formamide (DMF) at 0°C was added and then 18 ml phosphorus oxychloride was added dropwise under argon atmosphere until a coloured Vilsmeier salt completely precipitated. Next, the 9-hexyl-9H-carbazole solution (1.00 g, 4 mmol) in 10 ml DMF was added to a reaction mixture dropwise, while stirring at room temperature. The reaction mixture was stirred overnight at room

temperature. The reaction was poured into 100 ml ice-cold water and the pH was adjusted to close to alkaline by adding saturated sodium acetate solution. The solid product that collected was recrystallized from ethanol to produce brown crystals with 72% yield (0.88 g). M.p. 143–144°C; literature m.p. 144–146°C.<sup>[31]</sup>

### 2.3 | Synthesis of diethyl 2,2'-((9-hexyl-9H-carbazole-3,6-diyl)bis(methanylylidene))-bis(5-oxo-3-phenylthiazolidine-4,2-diylidene))bis(3-oxobutanoate) (CzPT)

In a 100 ml RB flask, 3,6-diformyl-N-hexylcarbazole (1) (0.92 g, 3 mmol) was dissolved in 40 ml ethanol. Ethyl-2-aceto-2-(5-oxo-3-phenylthiazolidin-2-ylidene)acetate (2) (1.83 g, 6 mmol) and three drops of piperidine were added. The reaction components were refluxed for 2 h and the product formed upon cooling was collected. Recrystallization of this solid was achieved from ethanol as golden crystals with 86% yield (2.27 g).

M.p. 211–212°C. Infrared (IR) (KBr): 3051 (C–H aromatic), 2946, 2879 (C–H aliphatic), 1726 (C=O), 1684 cm<sup>-1</sup> (broad, C=O). <sup>1</sup>H NMR (CDCl<sub>3</sub>): δ 0.81 (t, 3H, J = 7.00 Hz, CH<sub>3</sub>), 1.07–1.12 (m, 6H, –CH<sub>2</sub>CH<sub>2</sub>CH<sub>2</sub>–), 1.22 (t, J = 7.00 Hz, 6H, 2 CH<sub>3</sub>), 1.83 (m, 2H, CH<sub>2</sub>), 2.37 (s, 6H, 2 COCH<sub>3</sub>), 4.15 (q, J = 7.00 Hz, 4H, OCH<sub>2</sub>), 4.51 (t, J = 7.00 Hz, 2H, NCH<sub>2</sub>), 7.38–7.91 (m, 16H, Ar–H), 8.04 ppm (s, 2H, C=CH). Mass analysis (m/z, %): 882 (M<sup>+</sup>, 16.68), 590 (22.12), 479 (30.21), 454 (37.79), 434 (100.00), 401 (28.92), 368 (38.45), 279 (29.81), 128 (30.86), 116 (52.60), 68 (85.91). Analysis calculated for C<sub>50</sub>H<sub>47</sub>N<sub>3</sub>O<sub>8</sub>S<sub>2</sub> (882.06): C, 68.09; H, 5.37; N, 4.76%. Found: C, 68.28; H, 5.30; N, 4.87%.

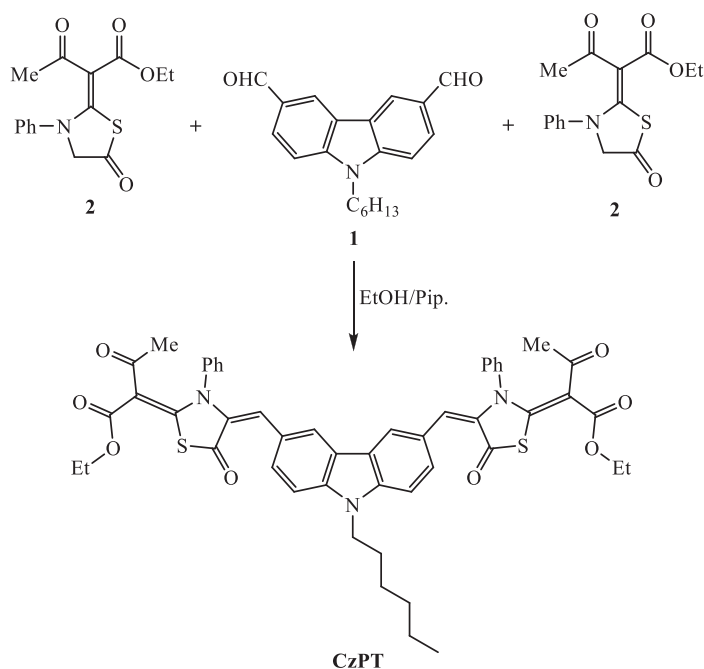
### 2.4 | Density functional studies

The Gaussian 09 W program<sup>[30]</sup> was used for quantum chemical calculations of the CzPT derivative at density functional theory (DFT) level with Becke3–Lee–Yang–Parr exchange–correlation functional (B3LYP)<sup>[31–33]</sup> and 6-311G<sup>++</sup> basis set. The obtained positive frequency values confirmed the stability of optimized geometry. The ground-excited state properties in hexane and DMF were studied using time-dependent DFT (TD-DFT)<sup>[34–36]</sup> at the B3LYP level in which the polarizable continuum model using integral equation formalism variant (IEF-PCM)<sup>[37,38,40]</sup> was used as a solvent model. Therefore, the obtained wavelengths were compared with that recorded experimentally in UV–visible spectra. Gauss-View<sup>[39]</sup> and Gauss-Sum 2.2<sup>[40]</sup> software were utilized for determination of HOMO–LUMO orbitals and electronic spectral contributions.

## 3 | RESULTS AND DISCUSSION

### 3.1 | Synthesis and structural elucidation of CzPT derivative

The synthetic pathway of a new carbazole-based thiazolidine-5-one compound (CzPT) is illustrated in Scheme 1. The formylated



*N*-hexyl-carbazole, 9-hexyl-9H-carbazole-3,6-dicarbaldehyde (**1**), was obtained according the standard Vilsmeier–Hack reaction protocol.<sup>[31]</sup> Furthermore, ethyl-2-aceto-2-(5-oxo-3-phenylthiazolidin-2-ylidene)acetate (**2**) was prepared with a 67% yield by nucleophilic addition of ethyl acetoacetate to phenyl isothiocyanate in DMF and KOH followed by *in situ* cyclization with chloroacetyl chloride as previously described in the literature.<sup>[43]</sup> In the final step, the target carbazole-based thiazolidine-5-one chromophore (**CzPT**) was obtained with a 86% yield using a modified Knoevenagel reaction. The reaction proceeded successfully by heating the precursor **1** with thiazolidine-4-one derivative **2** in ethanol and piperidine. Targeted organic dye was purified using recrystallization from ethanol. The structure of the newly synthesized chromophore (**CzPT**) was

confirmed by various spectroscopic techniques. The IR spectra showed absorptions at 1726 and 1684  $\text{cm}^{-1}$  related to carbonyl functions (C=O). The  $^1\text{H}$  NMR spectrum gave a triplet at  $\delta$  0.81 ppm for three protons ( $\text{CH}_3$ ), multiplet at  $\delta$  1.07–1.12 ppm for six protons ( $\text{CH}_2\text{CH}_2\text{CH}_2$ ), triplet at  $\delta$  1.21 ppm for six protons (two  $\text{CH}_3$ ), multiple at  $\delta$  1.78 ppm for two protons ( $\text{CH}_2$ ), singlet at  $\delta$  2.37 ppm (two  $-\text{COCH}_3$ ), quartet at  $\delta$  4.21 ppm for four protons (two  $-\text{OCH}_2$ ), and triplet at  $\delta$  4.51 for two protons ( $\text{NCH}_2$ ). The aromatic protons resonated as multiplet at  $\delta$  7.36–7.78 ppm, while olefinic protons resonated as singlet at  $\delta$  7.97 ppm (two  $\text{C}=\text{CH}$ ). Mass analysis displayed a molecular ion peak at  $m/z = 882.50$  (with relative intensity, 16.65%) related to the molecular formula  $\text{C}_{50}\text{H}_{47}\text{N}_3\text{O}_8\text{S}_2$ .

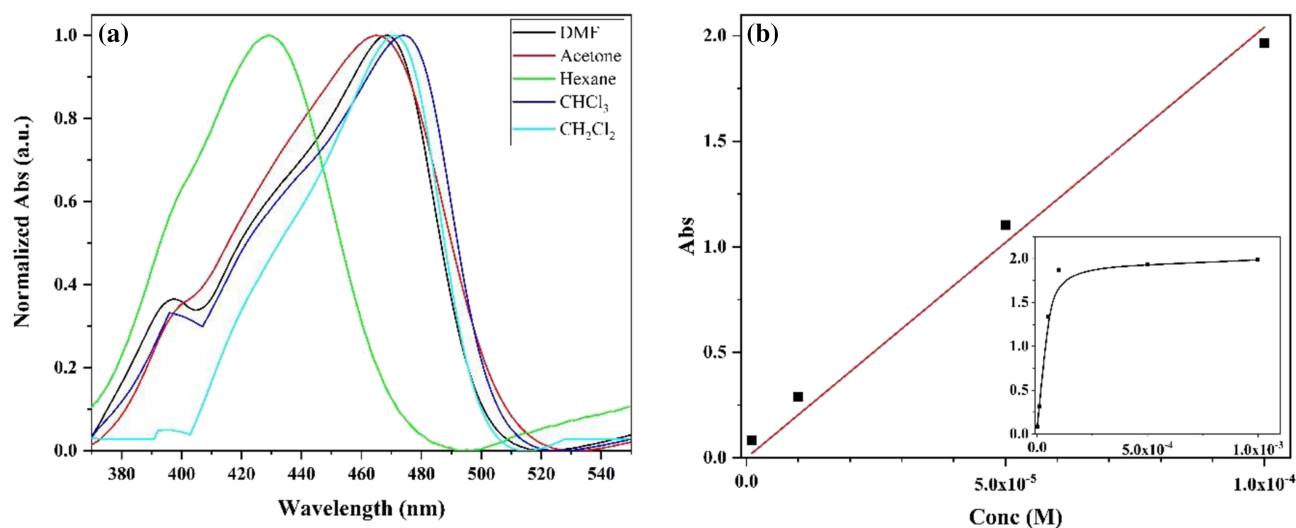


**FIGURE 1** Normalized UV-vis spectra of CzPT in different solvents (a) and linear fitting of absorbance-concentration plot (b)

### 3.2 | Absorption spectra and solvatochromism

**CzPT** UV-vis spectra,  $1 \times 10^{-4}$  M solution in different solvents, produced two bands, a weak one at 396–400 nm and a strong one,  $\lambda_{\text{max}} = 429\text{--}474$  nm. The first band was attributed to  $\pi\text{-}\pi^*$  transitions within conjugated aromatic moieties. While, the latter band was assigned to intramolecular charge transfer (ICT) that has  $\pi\text{-}\pi^*$  transition characteristics<sup>[41]</sup> which significantly enhanced its intensity (Figure 1a). At  $\lambda_{\text{max}}$ , the effect of **CzPT** solution concentration on absorbance, in chloroform, was studied in the range  $1 \times 10^{-6}$ – $1 \times 10^{-3}$  M. As shown in Figure 1b, absorbance increases reaching a plateau at  $1 \times 10^{-4}$  M after which Beer's law was not applicable. The linear fitting parameter exhibited a high molar extinction coefficient ( $\epsilon$ )  $2.04 \times 10^4$  L mol<sup>-1</sup> cm<sup>-1</sup>, obtained from the slope, with a good linear regression,  $r^2 = 0.9649$ . This deviation from Beer's law may be because the **CzPT** molecules underwent H-type aggregation. Such promoted aggregation was established by increasing the concentration in solution.<sup>[42]</sup> In addition, the molar extinction coefficients ( $\epsilon$ ) in different solvents ranged from  $2.62 \times 10^3$  L mol<sup>-1</sup> cm<sup>-1</sup> in n-hexane to  $2.04 \times 10^4$  L mol<sup>-1</sup> cm<sup>-1</sup> in chloroform (Table 1). The obtained high  $\epsilon$  values endorsed the suggested  $\pi\text{-}\pi^*$  characteristics of ICT transition ( $\lambda_{\text{max}}$ ) that originated from enhanced delocalization of electrons.<sup>[41,43]</sup>

Transition band type affected the absorption coefficient value and optical energy gap,  $E_g$ , which was determined by Tauc's equation<sup>[44]</sup>:

$$(\alpha h\nu) = B(h\nu - E_g)^r$$

where  $B$  is the energy independent constant and the exponent  $r = \frac{1}{2}$ , or 2, for direct or indirect conditions, respectively, and allowed transition band. The graphical representation of  $(\alpha h\nu)^r$  vs.  $(h\nu)$ , at different  $r$  values, was used to estimate  $E_g$  by extrapolating the linear portion of the curve to intercept the abscissa axis at  $r = 2$ . Therefore, the optical band gap could be estimated and was found to be in the range of 2.84–2.66 eV (Table 1). This value was low enough to reflect the ease of electronic transition between HOMO and LUMO levels. Therefore it led to relocation of electrons and left a hole due to facilitated electronic transitions. The values appeared to reflect the closeness of the optical and electronic bands, which is preferable for optical properties.<sup>[45]</sup>

The molecule that exhibited solvatochromism was differentially solvated in both ground and excited states. To explore the **CzPT** derivative solvatochromism, solvents with diverse polarity index were

used in absorption spectral measurements and the corresponding  $\lambda_{\text{max}}$  were recorded. The  $\lambda_{\text{max}}$  data showed a red shift with increasing polarity index from n-hexane to chloroform, 430 to 474 nm, respectively (Table 1). Using solvents with a higher polarity index, namely acetone and DMF, led to a blue shift, 465 and 468 nm, respectively. The difference in the maximum energy ( $E_{\text{max}}$ ) between the most polar and nonpolar solvent,  $\Delta E_{\text{max}}$ , was calculated to estimate the value and sign of solvatochromism (Table 1). The calculated  $\Delta E_{\text{max}}$  was +5.40 in which the positive sign is evidence that probe had red shifted and the **CzPT** ground state was less polar than the lowest excited state.<sup>[45]</sup>

The linear solvation-energy relationship (LSER) was applied to explore **CzPT** solvatochromism behaviour according to the next expression<sup>[46,47]</sup>:

$$(XYZ)_s = (XYZ)_0 + a\alpha + b\beta + c\pi^*$$

where  $(XYZ)_s$ ,  $(XYZ)_0$ ,  $\alpha$ ,  $\beta$  and  $\pi^*$  denote solvent absorption  $\lambda_{\text{max}}$  in cm<sup>-1</sup>, constant, hydrogen bond donor (HBD) or acidity, hydrogen bond acceptor (HBA) or basicity, and polarizability parameter based on  $\pi\text{-}\pi^*$  absorption of substituted aromatics,<sup>[48]</sup> respectively. The coefficients  $a$ ,  $b$ , and  $c$  are related coefficients for each polarity scale, respectively.

Multilinear regression showed good regression ( $r^2 = 0.9953$ ) with standard deviation (SD) 60.96. The values of absolute coefficients indicated that solvent HBD property,  $\alpha$ , is the most effective parameter in  $\lambda_{\text{max}}$ ,  $a = 1781.08$ . While, the solvent polarizability parameter,  $\pi^*$ , and solvent HBA became the second and third orders,  $c$  and  $b$  were 933.90 and 153.76, respectively (Table 2). Additionally, the HBD coefficient value was  $\sim 12$  times greater than that of the HBA coefficient. Therefore, the results clearly showed that multilinear regression described the **CzPT** solvatochromism origin.

### 3.3 | Fluorescence spectra

The **CzPT** fluorescence spectra in chloroform, concentration range  $1 \times 10^{-6}$  to  $5 \times 10^{-4}$  M, showed the effect of solution concentration on both intensity and maximum wavelength (Figure 2). Increasing the solution concentration led to a red shift of  $\lambda_{\text{em}}$  along with an intensity increase until it reached a maximum shift (10 nm) at  $1 \times 10^{-5}$  M concentration. At higher concentrations,  $> 1 \times 10^{-5}$  M, the  $\lambda_{\text{em}}$  shifted to higher

**TABLE 1** **CzPT** absorption  $\lambda_{\text{max}}$ , extinction coefficient ( $\epsilon$ ), maximum energy ( $E_{\text{max}}$ ) and absorption optical energy gap ( $E_{\text{g(Abs)}}$ ) in different solvents

Solvent	Polar index	$\epsilon_r$	$\mu$ (D)	$\lambda_{\text{max}}$ (nm)	$\epsilon$ (mol <sup>-1</sup> cm <sup>-1</sup> )	$E_{\text{max}}$ (kcal/mol)	$E_{\text{g(Abs)}}$ (eV)
Hexane	0.1	1.88	0.08	430	$2.62 \times 10^3$	66.49	2.66
CH <sub>2</sub> Cl <sub>2</sub>	3.1	8.93	1.14	471	$1.69 \times 10^4$	60.70	2.50
CHCl <sub>3</sub>	4.1	4.89	1.14	474	$1.87 \times 10^4$	60.32	2.48
Acetone	5.1	20.56	2.7	465	$1.14 \times 10^4$	61.49	2.48
DMF	6.4	36.71	3.81	468	$1.05 \times 10^4$	61.09	2.50

$\epsilon_r$  dielectric constant and  $\mu$  dipole moment.

Parameter	Absorption		Fluorescence	
	Value	Standard error ( $\pm$ )	Value	Standard error ( $\pm$ )
Intercept	22111.01	128.84	3311.96	249.53
$\alpha$	-1781.08	976.37	-4991.20	1891.03
$\beta$	153.76	301.42	-500.89	583.78
$\pi^*$	-933.90	105.36	-391.10	204.06
$r^2$	0.9953		0.9707	
SD	60.96		118.07	

**TABLE 2** The absorption and fluorescence spectra multilinear regression parameters

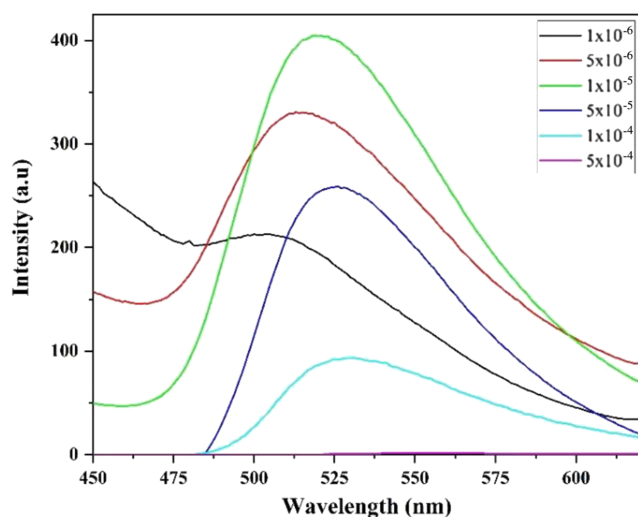


**FIGURE 2** Effect of CzPT concentration on the fluorescence performance in chloroform

wavelengths but was accompanied by a dramatic decrease in intensity. This behaviour may originate from excited molecules aggregating with unexcited molecules to form differently excited complexes, excimer or exciplex, which may or may not luminesce or luminesce at different frequencies compared with the monomeric excited molecule. Additionally, increasing the concentration led to a decrease in intermolecular mean distance and consequently molecule excitation energy was transmitted to adjacent molecules even as far as 100 nm.<sup>[42,49]</sup>

The fluorescence spectra of CzPT,  $1 \times 10^{-5}$  M, in solvents with different polarity displayed one peak that affected by solvent polarity (Figure 3). Stokes' shift, in  $\text{cm}^{-1}$ ,  $\Delta\bar{\nu} = \bar{\nu}_{\text{abs}} - \bar{\nu}_{\text{em}}$ , fundamentally originates from the structural relaxation of the molecular skeleton in the excited state. In general, the calculated Stokes' shift ( $\Delta\bar{\nu}$ ) of CzPT decreased with increasing polarity of the solvents, i.e. for less polar hexane,  $\Delta\bar{\nu} = 3801 \text{ cm}^{-1}$ , while in DMF it was  $2676 \text{ cm}^{-1}$  (Table 3).

The Lippert–Mataga equation was applied to interpret the spectral shifts of the CzPT derivative due to solvent molecule reorientation that was described by the solvent orientation polarizability parameter ( $\Delta f$ ) and expressed by this equation<sup>[50]</sup>:

$$\Delta\bar{\nu} = \bar{\nu}_a - \bar{\nu}_f = \frac{2(\mu_e - \mu_g)^2}{hca^3} (\Delta f) + \text{constant } \Delta f = \left( \frac{\epsilon_r - 1}{2\epsilon_r + 1} \right) - \left( \frac{n^2 - 1}{2n^2 + 1} \right)$$

where  $\Delta\bar{\nu}$  is Stokes' shift ( $\text{cm}^{-1}$ ),  $\mu_e$  is the excited state dipole,  $\mu_g$  is the ground state dipole,  $h$  is Planck's constant,  $c$  is the velocity of

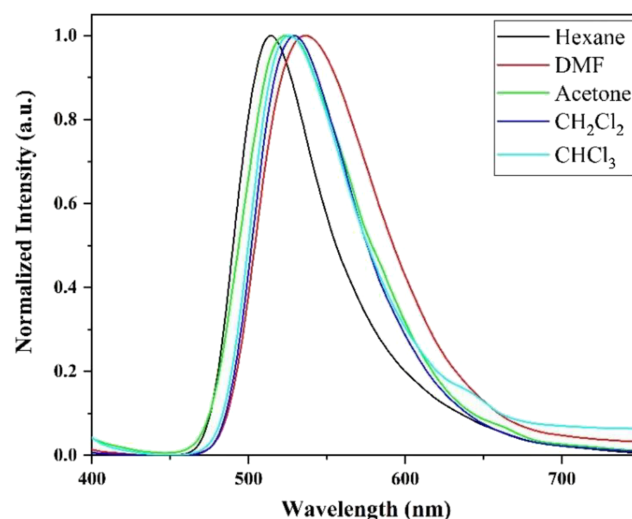


**FIGURE 3** Normalized fluorescence spectra of CzPT,  $1 \times 10^{-5}$  M, in different solvents

light in vacuum,  $a$  is solvent cavity (Onsager cavity radius),  $\epsilon_r$  is the dielectric constant and  $n$  is the refractive index.

The Lippert–Mataga plot,  $\Delta\bar{\nu}$  versus  $\Delta f$ , exhibited poor linearity, with a regression coefficient ( $r^2$ ) of 0.5087, neglecting n-hexane (Figure 4a). This poor linear regression coefficient suggested that Lippert–Mataga did not account for additional factors such as fluorophore hydrogen bonding and ICT.<sup>[51]</sup>

To overcome Lippert–Mataga shortages, the LSER, as shown in the following equation,<sup>[46,47]</sup> was employed to describe the CzPT–solvent interaction and its effect on Stokes' shifts:

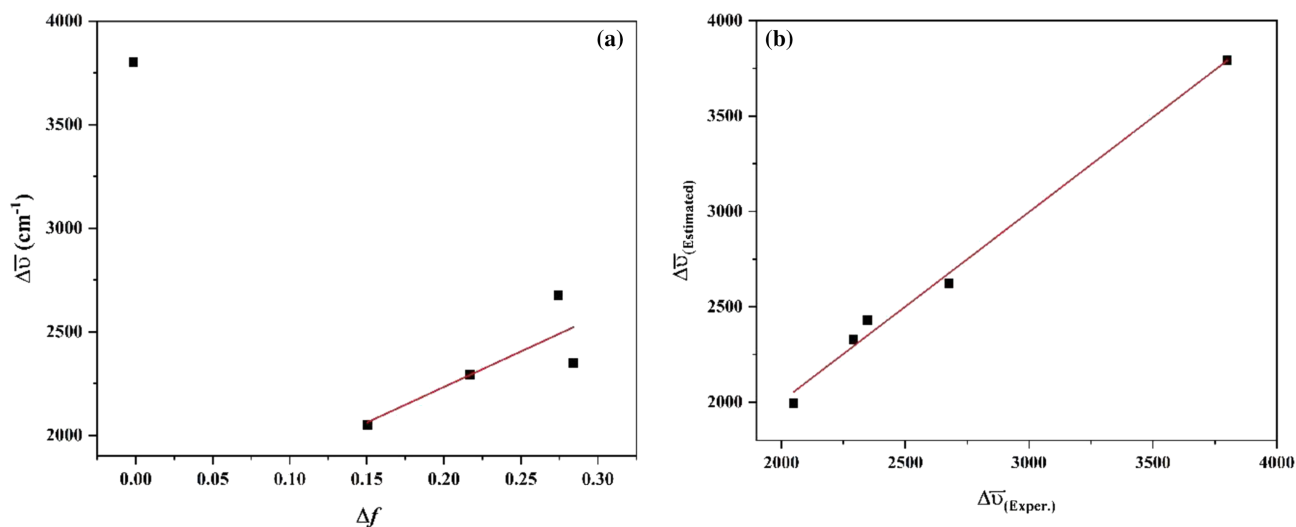
$$(XYZ)_s = (XYZ)_0 + a\alpha + b\beta + c\pi^*$$

where  $(XYZ)_s$  is the Stokes' shift, and other parameters  $(XYZ)_0$ ,  $\alpha$ ,  $\beta$ ,  $\pi^*$ ,  $a$ ,  $b$ , and  $c$ <sup>[48]</sup> have been described before.

The solvent Stokes' shift showed a good regression coefficient ( $r^2 = 0.9707$ ) compared with the Lippert–Mataga plots and the obtained coefficients were displayed in Table 2. The coefficients absolute value revealed that the Stokes' shifts were affected greatly by the solvent hydrogen bond donating capability, HBD, or acidity in which the HBA or basicity comes in the second position. Additionally, the HBD coefficient absolute value,  $a$ , was  $\sim 10$  and was 13 times higher than that of HBA and the dipolarity/polarizability,  $b$  and  $c$ , respectively.

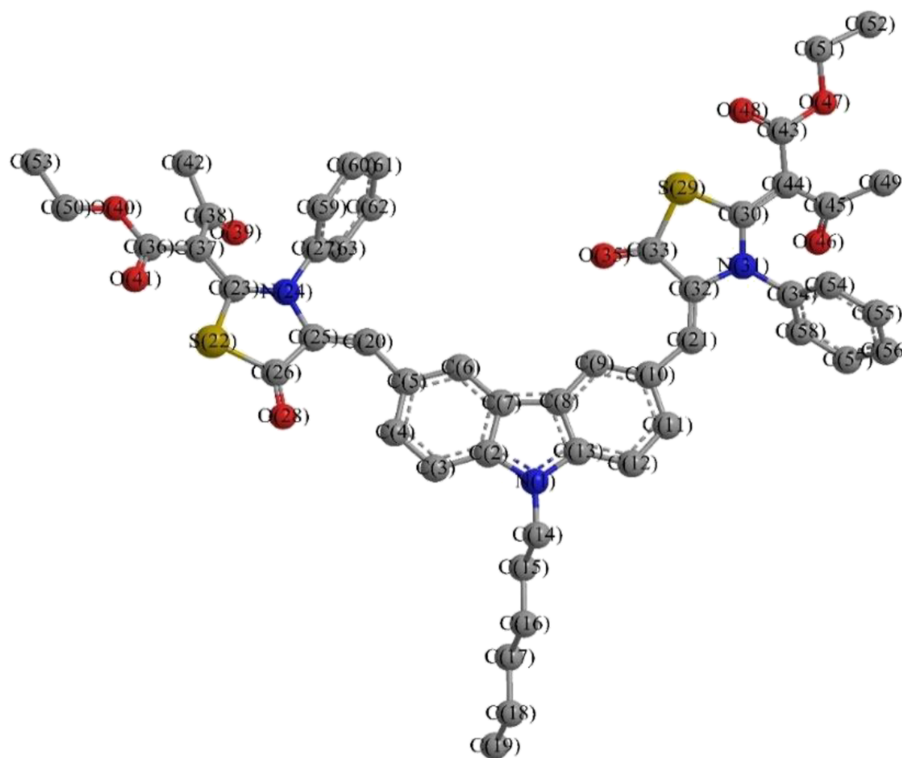
**TABLE 3** CzPT maximum  $\lambda_{em}$ , Stokes' shift ( $\Delta\bar{\nu}$ ), emission optical energy gap ( $E_{g(em)}$ ), quantum yield ( $\phi_f$ ) and solvents orientation polarizability ( $\Delta f$ )

Solvent	$\Delta f$	$\alpha$	$\beta$	$\pi^*$	$\lambda_{em}$ (nm)	$\Delta\bar{\nu}$ ( $cm^{-1}$ )	$\phi_f$	$E_{g(em)}$
Hexane	-0.0014	0	0	-1.23	528	3801	0.728	2.41
CH <sub>2</sub> Cl <sub>2</sub>	0.2171	0.13	0.1	0.73	535	2292	0.776	2.35
CHCl <sub>3</sub>	0.1504	0.2	0.1	0.69	522	2049	0.825	2.36
Acetone	0.2841	0.08	0.48	0.62	528	2348	0.662	2.38
DMF	0.2744	0	0.69	0.88	522	2676	0.628	2.32

**FIGURE 4** (a) Lippert-Mataga plot of  $\Delta\bar{\nu}$  vs.  $\Delta f$ ; (b) linear relationship between experimental and predicted  $\Delta\bar{\nu}$  of CzPT

To examine LSER quality, the predicted Stokes' shifts, obtained using the estimated parameters from LSER, were correlated graphically to the experimental values as displayed in Figure 4b. A good

linear relationship was obtained that had slope and regression coefficient values almost at unity, with slope = 0.9927 and  $r^2 = 0.9902$ , respectively. Therefore, the solvatochromic origin of

**FIGURE 5** The CzPT optimized structure in hexane (H atoms were hidden for clarity)

the CzPT derivative was explained using the multilinear regression model.

Finally, CzPT relative quantum yield ( $\phi$ ) in different solvents was assessed by quinine sulfate in 0.1 M H<sub>2</sub>SO<sub>4</sub> as standard.<sup>[52]</sup> As shown in Table 3, quantum yield increased when increasing the solvent polarity and reached a maximum in CHCl<sub>3</sub> of 0.825, after which it

decreased in highly polar solvents to reach 0.628 in DMF, the most polar solvent.

### 3.4 | Computational aspects

#### 3.4.1 | Quantum chemical studies

The CzPT derivative was optimized in the gaseous state and then in hexane and DMF as solvent to study the solvent effect using DFT quantum chemical calculations. In gaseous and solvated states, the CzPT optimized structures have almost planar configuration in which the carbazole and thiazolidinone moieties were co-planar. Both phenyl rings and oxobutanoate groups were perpendicular and tilted with respect to the carbazole plane, respectively (Figure 5). Complete lists of DFT obtained bond length, bond angle and dihedral angles are shown in Tables S1–S3.

Frontier molecular orbitals, HOMO and LUMO, have noteworthy roles in understanding ICT.<sup>[53–55]</sup> HOMO revealed the electron donation ability, which appeared to spread over electron-rich moieties, while LUMO presented electron acceptability, which appeared localized on electron-deficient moieties.<sup>[56]</sup> The gaseous and solvated frontier orbitals 3D-plots demonstrated HOMO were concentrated mainly on  $\pi$ -orbitals of carbazole and heteroatoms of thiazolidinone and oxobutanoate groups, while LUMO were concentrated on  $\pi^*$ -orbitals of these moieties. The red and green colours were designated as wave function positive and negative phases<sup>[57]</sup> (Figure 6).

In the gaseous state,  $E_{\text{HOMO}}$  and  $E_{\text{LUMO}}$  were  $-5.63$  and  $-4.03$  eV, respectively, with an exhibited energy gap of  $\Delta E_{\text{H-L}} = 1.60$  eV. In the solvated state, hexane solvation led to a slight decrease in both  $E_{\text{HOMO}}$  and  $E_{\text{LUMO}}$ , by 0.03 eV and so the energy gap was maintained at 1.60 eV. In contrast, DMF solvation led to an increase in  $E_{\text{HOMO}}$  and  $E_{\text{LUMO}}$ , with respect to the gaseous state, and were  $-5.72$  and  $-4.15$  eV, respectively, but  $\Delta E_{\text{H-L}}$  was slightly

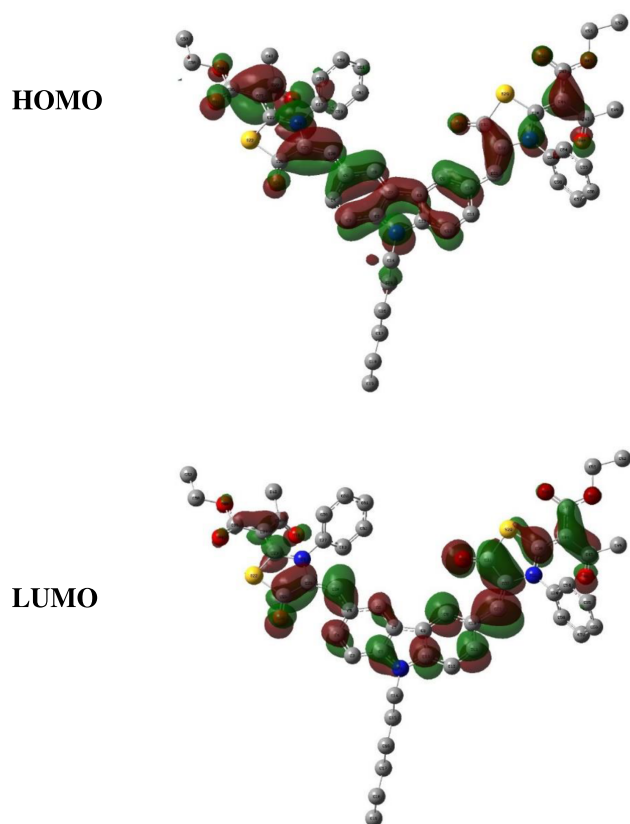


FIGURE 6 Frontier HOMO and LUMO of CzPT in gaseous state

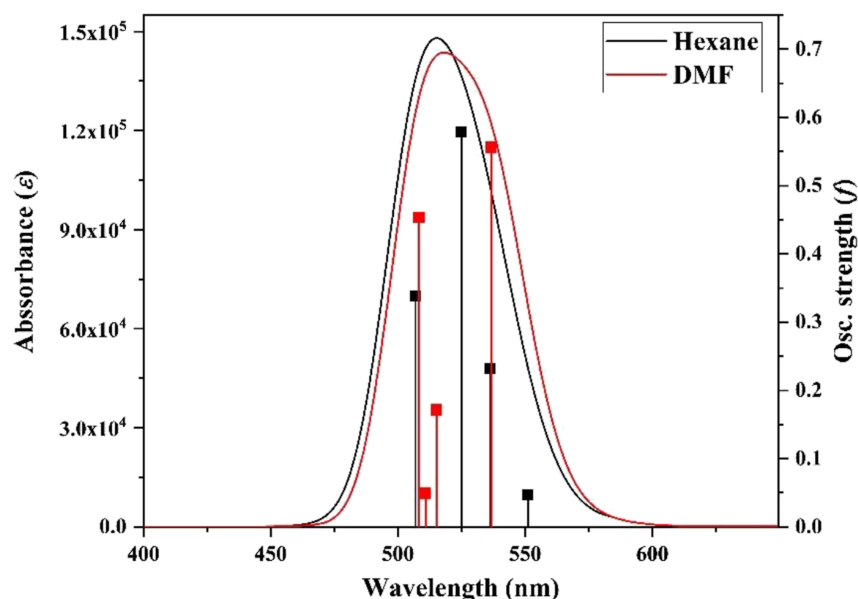


FIGURE 7 TD-DFT electronic spectra of CzPT in hexane and DMF

changed (1.58 eV). Hexane slightly stabilized both molecular orbitals, while DMF de-stabilized both, which may suggest that HOMO and LUMO have almost the same degree of polarity.

The generated TD-DFT electronic spectra of **CzPT** in hexane and DMF showed one band at 515 and 520 nm, respectively (Figure 7). The DFT calculated band resulted from the overlapping of many transitions, as shown in Table 4. The data indicated transitions at 525 and 537 nm in hexane and DMF, respectively, which mainly originated from HOMO→LUMO transitions with highest oscillator strength, 0.578 and 0.556, and contribution, 83% and 91%, respectively. Moreover, the molecular orbitals HOMO, HOMO-1, and HOMO-2 were the donors, while only LUMO and LUMO+1 were the acceptors in other electronic transitions at long or shorter wavelengths. Finally, the comparison of experimental data with TD-DFT electronic spectra, revealed the presence of a calculated  $\lambda_{\text{max}}$  band at higher wavelengths than the experimental, which may be because the TD-DFT calcula-

tions did not account for the effect of spin-orbit coupling and molecular vibrational motion.<sup>[58,59]</sup>

### 3.4.2 | Crystal shape effect

Hirshfeld demonstrated a procedure to put the closest model of a crystal inside a crystal packing system using Crystal explorer software 3.1.<sup>[60]</sup> The **CzPT** derivative was adjusted using the VESTA package to be suitable for crystal building.<sup>[61]</sup> A 3D-model of the compound was optimized first and the crystal was established through normalized contact distance ( $d_{\text{norm}}$ ) and curvedness types (Figure 7). The model of  $d_{\text{norm}}$  type differentiates the contact features between molecular surfaces in crystal packing by colour indicators. Red, white, and blue colours, refer to strong, moderate, and weak interactions, respectively. The strength of contact depends on the length of H-bonding between surfaces, according to van der Waals radii. The short distance depicted by red spot points to strong contact, while blue and white point to long and moderate lengths, respectively. Several red spots surround oxygen atoms and reflect the significant role of oxygen atoms in contact preferences between neighbouring crystals inside packing. Furthermore, the curvedness type divided the surface into several portions suitable for contact. Side chains may prevent perfect contact between the closest crystals and packing may be yielded with many imperfections.<sup>[62]</sup> It is known that the crystal features and geometry of a compound determine its physicochemical properties, particularly its photophysical properties during electron transfer processes.<sup>[63]</sup> The unit cell was demonstrated via the VESTA package to visualize the most fitted shape of unit cell that seemed to be a face-centred cubic shape (Figure 8). The volume of the unit cell was 15 059.2 Å<sup>3</sup>,  $a = b = c = 24.6945$  Å and  $\alpha = \beta = \gamma = 90^\circ$ . In addition, the X-ray diffraction (XRD) pattern was obtained using Crystal Maker software (Figure 9) to determine d-spacing (0.10 Å) and particle size (24.69 Å). Small d-spacing between the inner levels in the crystal, may lead to subsequent emission of light at a lower energy levels and causes photophysical properties. Also, the reduced uniformity of the crystal feature may lead to dislocation or anomalous arrangement of crystals with irregular spacing, which automatically enhance the optical properties of such crystals.

**TABLE 4** TD-DFT absorption electronic transitions of **CzPT** in hexane and DMF

Transition (nm)	Osc. strength	Major contributions
Hexane		
551	0.046	HOMO-2→LUMO (96%)
536	0.232	HOMO-2→LUMO+1 (78%), HOMO-1→LUMO+1 (19%)
525	0.578	HOMO→LUMO (83%)
507	0.338	HOMO-1→LUMO (43%), HOMO→LUMO+1 (43%)
DMF		
537	0.556	HOMO→LUMO (91%)
515	0.171	HOMO-1→LUMO+1 (82%)
511	0.049	HOMO-2→LUMO+1 (27%), HOMO-1→LUMO (32%), HOMO→LUMO+1 (31%)
508	0.453	HOMO-1→LUMO (49%), HOMO→LUMO+1 (51%)

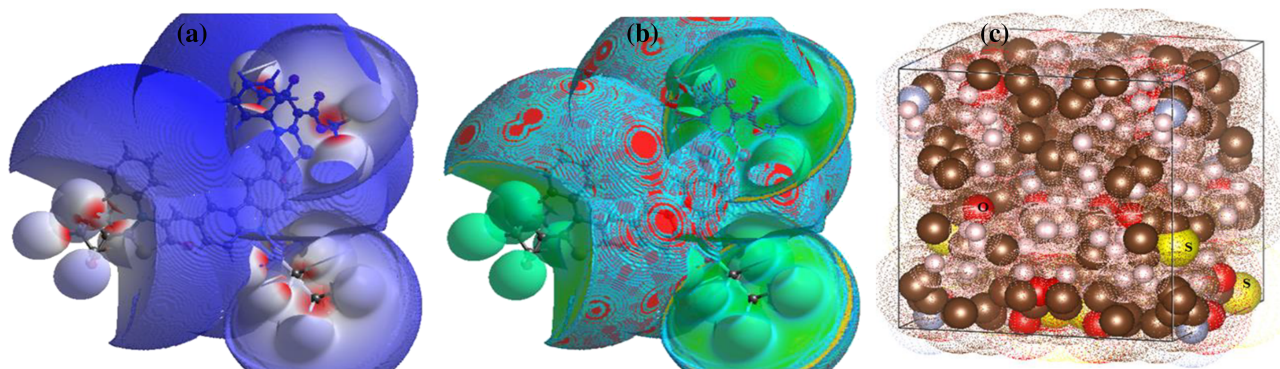


**FIGURE 8**  $d_{\text{norm}}$  (a), curvedness (b) and unit cell (c) of **CzPT** compound

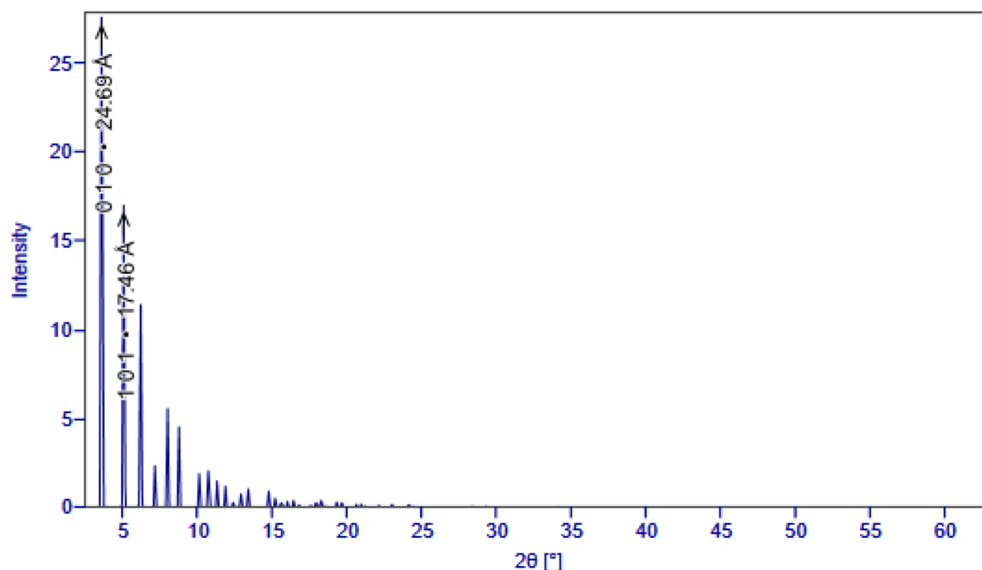


**FIGURE 9** Theoretical XRD pattern of CzPT compound

## 4 | CONCLUSION

A new chromophore, 3,6-bis(thiazolidin-5-one-2-yl)carbazole (CzPT) was obtained from the condensation of 3,6-diformyl-N-hexylcarbazole with 2 moles of ethyl-2-aceto-2-(5-oxo-3-phenylthiazolidin-2-ylidene)acetate. The UV-vis absorption spectra in different solvents were generated and showed two absorption bands due to conjugated aromatic moieties localized at  $\pi$ - $\pi^*$  transitions and ICT. The effect of solvent polarity on the spectroscopic behaviour of the CzPT derivative was monitored using different solvents. Additionally, a small bathochromic shift in photophysical properties indicated minor H-type aggregation in the CzPT structure with increasing solvent polarity. Furthermore, DFT/B3LYP geometry optimization and electronic configurations of CzPT were studied and indicated its nonplanar structure. Crystal shape and defects in the unit cell may lead to significant optical characteristics for the CzPT crystal.

### ORCID

Ismail Althagafi  <https://orcid.org/0000-0002-9343-2595>

Nashwa El-Metwaly  <https://orcid.org/0000-0002-0619-6206>

### REFERENCES

- [1] D. Prochowicz, A. Kornowicz, J. Lewiński, *Chem. Rev.* **2017**, *117*, 13461.
- [2] H. Nakanotani, T. Higuchi, T. Furukawa, K. Masui, K. Morimoto, M. Numata, H. Tanaka, Y. Sagara, T. Yasuda, C. Adachi, *Nat. Commun.* **2014**, *5*, 1.
- [3] R. Meerheim, K. Walzer, G. He, M. Pfeiffer, K. Leo, *Int. Soc. Opt. Photonics* **2006**, 6192, 1.
- [4] S. Reineke, F. Lindner, G. Schwartz, N. Seidler, K. Walzer, B. Lüssem, K. Leo, *Nature* **2009**, 459, 234.
- [5] A. Zampetti, A. Minotto, F. Cacialli, *Adv. Funct. Mater.* **2019**, *29*, 1807623.
- [6] Q. Wei, Z. Ge, B. Voit, *Macromol. Rapid Commun.* **2019**, *40*, 1800570.
- [7] S. S. Palayangoda, X. Cai, R. M. Adhikari, D. C. Neckers, *Org. Lett.* **2008**, *10*, 281.
- [8] I. Aharonovich, D. Englund, M. Toth, *Nat. Photonics* **2016**, *10*, 631.
- [9] Z. Li, Y. Q. Dong, J. W. Lam, J. Sun, A. Qin, M. Häußler, Y. P. Dong, H. H. Sung, I. D. Williams, H. S. Kwok, *Adv. Funct. Mater.* **2009**, *19*, 905.
- [10] W. Guo, B. J. Engelman, T. L. Haywood, N. B. Blok, D. S. Beaudoin, S. O. Obare, *Talanta* **2011**, *87*, 276.
- [11] J. R. Huth, R. Mendoza, E. T. Olejniczak, R. W. Johnson, D. A. Cothron, Y. Liu, C. G. Lerner, J. Chen, P. J. Hajduk, *J. Am. Chem. Soc.* **2005**, *127*, 217.
- [12] J. N. Wilson, E. T. Kool, *Org. Biomol. Chem.* **2006**, *4*, 4265.
- [13] H. Kobayashi, M. Ogawa, R. Alford, P. L. Choyke, Y. Urano, *Chem. Rev.* **2010**, *110*, 2620.
- [14] Z. Zeng, R. Ma, C. Liu, Y. Xu, H. Li, F. Liu, S. Sun, *Sens. Actuat. B Chem.* **2017**, *250*, 267.
- [15] R. Pinalli, A. Pedrini, E. Dalcanale, *Chem. Soc. Rev.* **2018**, *47*, 7006.
- [16] C. Filippi, M. Zaccheddu, F. Buda, *J. Chem. Theory Comput.* **2009**, *5*, 2074.
- [17] S. A. Nizar, T. Kobayashi, F. B. M. Suah, *Luminescence* **2020**, *35*(8), 1286.
- [18] J. Tagare, N. Verma, K. Tarafder, S. Vaidyanathan, *Luminescence* **2020**, *35*(8), 1338.
- [19] C. Wang, J. Xu, H. Li, W. Zhao, *Luminescence* **2020**, *35*(8), 1373.
- [20] I. Constantinoiu, C. Viespe, *Sensors* **2020**, *20*(18), 5118.
- [21] R. B. Priya, T. Venkatesan, G. Pandiyarajan, H. M. Pandya, *J. Environ. Nanotechnol.* **2015**, *4*, 15.
- [22] O. Brede, A. Maroz, R. Hermann, S. Naumov, *J. Phys. Chem. A* **2005**, *109*, 8081.
- [23] C. H. Yang, S. H. Liao, Y. K. Sun, Y. Y. Chuang, T. L. Wang, Y. T. Shieh, W. C. Lin, *J. Phys. Chem. C* **2010**, *114*, 21786.
- [24] J. Zhang, W. Chen, S. Kalytchuk, K. F. Li, R. Chen, C. Adachi, Z. Chen, A. L. Rogach, G. Zhu, P. K. Yu, *ACS Appl. Mater. Interfaces* **2016**, *8*, 11355.
- [25] S. J. Pond, O. Tsutsumi, M. Rumi, O. Kwon, E. Zojer, J. L. Brédas, S. R. Marder, J. W. Perry, *J. Am. Chem. Soc.* **2004**, *126*, 9291.
- [26] H. Sakamoto, T. Yamamura, K. Takumi, K. Kimura, *J. Phys. Org. Chem.* **2007**, *20*, 900.
- [27] A. Hennig, H. Bakirci, W. M. Nau, *Nat. Methods* **2007**, *4*, 629.
- [28] M. Dekhtyar, W. Rettig, A. Rothe, V. Kurdyukov, A. Tolmachev, *J. Phys. Chem. A* **2019**, *123*, 2694.
- [29] H. Shi, M. Li, D. Xin, L. Fang, J. Roose, H. Peng, S. Chen, B. Z. Tang, *Dyes Pigment.* **2016**, *128*, 304.

- [30] M. Frisch, G. Trucks, H. Schlegel, G. Scuseria, M. Robb, J. Cheeseman, G. Scalmani, V. Barone, B. Mennucci, G. Petersson, Gaussian 09, Revision A. 1, Wallingford, CT, USA: Gaussian, 2009.
- [31] A. D. Becke, *J. Chem. Phys.* **1993**, *98*, 5648.
- [32] C. Lee, W. Yang, R. G. Parr, *Phys. Rev. B* **1988**, *37*, 785.
- [33] J. P. Perdew, Y. Wang, *Phys. Rev. B* **1992**, *46*, 12947.
- [34] R. Bauernschmitt, R. Ahlrichs, *Chem. Phys. Lett.* **1996**, *256*, 454.
- [35] R. E. Stratmann, G. E. Scuseria, M. J. Frisch, *J. Chem. Phys.* **1998**, *109*, 8218.
- [36] M. E. Casida, C. Jamorski, K. C. Casida, D. R. Salahub, *J. Chem. Phys.* **1998**, *108*, 4439.
- [37] M. Cossi, V. Barone, *J. Chem. Phys.* **2001**, *115*, 4708.
- [38] M. Cossi, N. Rega, G. Scalmani, V. Barone, *J. Comput. Chem.* **2003**, *24*, 669.
- [39] R. Dennington, T. Keith, J. Millam, GaussView, version 5, Semichem Inc., Shawnee Mission, KS, 2009.
- [40] N. M. O'boyle, A. L. Tenderholt, K. M. Langner, *J. Comput. Chem.* **2008**, *29*, 839.
- [41] W. I. Hung, Y. Y. Liao, C. Y. Hsu, H. H. Chou, T. H. Lee, W. S. Kao, J. T. Lin, *Chem. – Asian J.* **2014**, *9*, 357.
- [42] J. C. Lindon, G. E. Tranter, D. Koppenaal, *Encyclopedia of spectroscopy and spectrometry*, Academic Press, Oxford, UK **2016**.
- [43] X. Liu, J. Long, G. Wang, Y. Pei, B. Zhao, S. Tan, *Dyes Pigm.* **2015**, *121*, 118.
- [44] J. Tauc, *Amorphous and liquid semiconductors*, Springer Science & Business Media, Springer, New York **2012**.
- [45] H. Park, S. K. Chang, *Dyes Pigm.* **2015**, *122*, 324.
- [46] F. Han, L. Chi, W. Wu, X. Liang, M. Fu, J. Zhao, *J. Photochem. Photobiol., a* **2008**, *196*, 10.
- [47] S. Azizi, M. Chaichi, M. Yousefi, *Spectrochim. Acta A* **2009**, *73*, 101.
- [48] C. Reichardt, T. Welton, *Solvents and solvent effects in organic chemistry*, 4th ed., John Wiley & Sons, Germany **2011**.
- [49] M. F. Al-Kadhemy, I. F. Alsharuee, A. A. D. Al-Zuky, *J. Physiol. Sci.* **2011**, *22*, 77.
- [50] B. Valeur, M. Berberan-Santos, *Mol. Fluoresc. Princip. Appl.* **2001**, *2*, 56.
- [51] Z. Li, Q. Yang, R. Chang, G. Ma, M. Chen, W. Zhang, *Dyes Pigm.* **2011**, *88*, 307.
- [52] H. J. Yvon, Horiba Jobin Yvon Inc.: Middlesex, UK, **2012**.
- [53] S. Xavier, S. Periandy, S. Ramalingam, *Spectrochim. Acta A* **2015**, *137*, 306.
- [54] M. M. Makhlof, A. S. Radwan, B. Ghazal, *Appl. Surf. Sci.* **2018**, *452*, 337.
- [55] A. Bouchoucha, S. Zaater, S. Bouacida, H. Merazig, S. Djabbar, *J. Mol. Struct.* **2018**, *1161*, 345.
- [56] F. A. Bulat, E. Chamorro, P. Fuentealba, *J. Phys. Chem. A* **2004**, *108*, 342.
- [57] V. Arjunan, P. Balamourougane, M. Kalaivani, A. Raj, S. Mohan, *Spectrochim. Acta A*, **2012**, *96*, 506.
- [58] M. Karabacak, E. Kose, A. Atac, *Spectrochim. Acta A* **2012**, *91*, 83.
- [59] J. P. Holland, P. J. Barnard, S. R. Bayly, J. R. Dilworth, J. C. Green, *Inorg. Chim. Acta* **2009**, *362*, 402.
- [60] M. J. Turner, J. J. McKinnon, D. Jayatilaka, M. A. Spackman, *Cryst. Eng. Comm.* **2011**, *13*, 1804.
- [61] K. Momma, F. Izumi, *J. Appl. Crystallogr.* **2011**, *44*, 1272.
- [62] S. Roy, N. Hari, S. Mohanta, *Eur. J. Inorg. Chem.* **2019**, *29*, 3411.
- [63] N. Amiri, M. Hajji, T. Roisnel, G. Simonneaux, H. Nasri, *Res. Chem. Intermed.* **2018**, *44*, 5583.

#### SUPPORTING INFORMATION

Additional supporting information may be found online in the Supporting Information section at the end of this article.

**How to cite this article:** Bawazeer TM, Althagafi I, Morad M, et al. Luminescence feature of new 3,6-di(thiazolidin-5-one-2-yl)-carbazole derivative: synthesis, photophysical properties, density functional theory studies, and crystal shape effect. *Luminescence*. 2021;36:904–913. <https://doi.org/10.1002/bio.4013>